JOURNAL OF CATALYSIS **178,** 119–136 (1998)
ARTICLE NO. CA982132

Molybdenum Nitride and Carbide Prepared from Heteropolyacid

III. Hydrodesulfurization of Benzothiophene

Senzi Li and Jae Sung Lee[1]

Department of Chemical Engineering and School of Environmental Engineering, Pohang University of Science and Technology, Pohang, 790-784, Republic of Korea

Received October 31, 1997; revised April 30, 1998; accepted April 30, 1998

Hydrodesulfurization (HDS) of benzothiophene has been studied over molybdenum nitride prepared from MoO_3, 12-molybdophosphoric acid (HPA), and $MoO_3 + P_2O_5$ (a physical mixture of P_2O_5 and MoO_3 with stoichiometry of P to Mo equal to that of HPA). It was observed that Mo_2N was an effective catalyst for HDS of benzothiophene. Ethylbenzene was the exclusive product over the whole temperature range investigated. Adding P_2O_5 to the precursor MoO_3 had beneficial effects on HDS of benzothiophene. Most importantly, the presence of phosphorus in Mo_2N dramatically improved its resistance against catalyst deactivation. The reaction pathway of HDS appeared not to be changed by adding phosphorus. Adsorption, XRD, EPMA, and XPS characterized the catalysts after HDS reaction. The bulk structure of face-centered-cubic Mo_2N and its morphology were retained after HDS reaction. However, the presence of phosphorus in the precursors resulted in growing polycrystallinity and amorphism in produced Mo_2N. A great amount of sulfur compounds was found deposited on the surface of the catalysts after reaction, leading to catalyst deactivation. The presence of phosphorus in Mo_2N reduced the amount of deposited sulfur compounds that appeared responsible for the improved resistance against the catalyst deactivation.

Key Words: **hydrodesulfurization; phosphorus-containing Mo_2N; promotional effect; deactivation.**

INTRODUCTION

Hydrodesulfurization (HDS) is the most important and extensively investigated hydrotreating process compared to hydrodenitrogenation (HDN), hydrodeoxygenation (HDO), and hydrodemetallization (HDM). In industrial processes, molybdenum sulfides promoted with cobalt or nickel and supported on γ-Al_2O_3 are usually used as catalysts (1–4). Phosphorus is introduced to the catalysts as a promoter (5–17). It has been reported that the presence of phosphorus improves Mo dispersion (18–20), modifies the acid strength distribution (21), promotes the formation of active species MoS_2 and decreases its agglomeration (22). However, many aspects of catalyst structure and reaction mechanism are still uncertain, although a number of explanations have been proposed (23–26). Moreover, the effect of phosphorus has yet to be clearly elucidated.

Since a temperature-programmed method was employed to synthesize unsupported Mo_2N with high specific surface areas (27–29), a variety of reactions, including HDS and HDN, have been studied over molybdenum nitride and carbide catalysts, and some encouraging results have been obtained (30–36). It has been reported that molybdenum nitride possesses high activity for thiophene HDS (34) and that Mo_2N is more active than MoS_2 for the conversion of pyridine and quinoline, but it is less active than the sulfide for HDS of coal-derived naphtha (37, 38). Nevertheless, compared to thiophene and dibenzothiophene, there are fewer studies investigating HDS of benzothiophene over molybdenum nitride. Furthermore, to the best of our knowledge, no report concerns the effect of introducing phosphorus to Mo_2N catalysts on their catalytic behaviors in HDS and HDN reaction.

The present study is based on and is an extension of our preceding investigations (39, 40). We are motivated by the observation that molybdenum nitride is an active catalyst in HDN of indole and its initial activity is considerably improved by the presence of phosphorus (40). The purpose of this study is to investigate the activity of HDS of benzothiophene over the three Mo_2N catalysts with and without phosphorus as described in the previous papers (39, 40). An attempt is made to gain more insight into the role of phosphorus in HDS reaction. Moreover, the activity of HDS is compared with that of HDN in order to get a better understanding of the active sites and the cause of deactivation.

EXPERIMENTAL

Catalyst Preparation

All of the catalysts were prepared by a temperature-programmed reaction method, and the detailed synthesis

[1] To whom all correspondence should be addressed. E-mail: jlee@postech.ac.kr.

0021-9517/98 $25.00

procedure have been described in the previous papers (39, 40). Typically, the stoichiometric amount of precursor was employed to produce 0.005 mol Mo_2N. Three precursors, $H_3PMo_{12}O_{40}26H_2O$ (Junsei, 99.95%), denoted as HPA throughout this paper, MoO_3 powder (Aldrich, 99.95%), or a physical mixture (ground with a mortar and a pestle) of MoO_3 and P_2O_5 (Janssen, 99%) with stoichiometry of P to Mo equal to that of HPA, denoted as $MoO_3 + P_2O_5$, was loaded in U-shaped quartz reaction cell stuffed with quartz wool at the bottom to hold the powders. A stream of NH_3 (Matheson, 99.99%) at a flow rate of 150 μmol s^{-1} was passed through the reaction cell at atmospheric pressure. Temperature of the preparation was increased linearly at a rate of 30 K h^{-1} from 573 to 973 K. All materials were synthesized at atmospheric pressure.

Hydrodesulfurization of Benzothiophene

Benzothiophene (hereafter abbreviated as BTP), representative of sulfur compounds in the crude oil, was chosen as the model material to test HDS activity of the catalysts. Unless otherwise indicated, the reaction was conducted by the following procedure. Each batch of 0.005 mol Mo_2N catalysts (1.03 g) prepared from different precursors as described above was used for the catalytic reaction. The hydrodesulfurization of BTP was carried out *in situ* without exposing the catalysts to air after preparation. The catalysts were pretreated under a flow of hydrogen (15 μmol s^{-1}) at 673 K for 1 h prior to the delivery of BTP. Benzothiophene (Aldrich, 99%) was introduced into a flow of hydrogen (90 μmol s^{-1}) via a syringe pump (Saga Instruments) at a pumping rate of 0.1 cm^3 h^{-1} at atmospheric pressure. A vaporization chamber filled with glass beads was positioned upstream of quartz reactor to ensure a complete mixing of gases. Identification and analysis of reaction products were carried out by an on-line HP 5890 gas chromatography (GC) equipped with an FID detector and by mass spectrometer (HP 5972 MSD). An STB-1 capillary column (60 m $\times$ 0.25 mm $\times$ 0.25 μm) of Supelco was used to separate products for GC analysis.

The hydrodesulfurization of BTP as a function of reaction temperature was performed following a temperature ramping program from 573 to 723 K. Unless otherwise mentioned, the temperature was maintained at the indicated temperature for 2 h prior to moving to the next temperature level at a ramping rate of 0.083 K s^{-1}. The effluent products were analyzed every 20 min via a six-port sampling valve attached on GC. The average value of the last three samplings was taken as rate data of the indicated temperature since deactivation occurred with time on stream.

Characterization of Catalysts

Since fresh molybdenum carbide and nitride were burned violently with flame upon exposure to air, the samples were passivated prior to the characterization measurements by letting air diffuse slowly into the reaction cell with one end of the reactor open to the atmosphere for 10 h and causing a mild surface oxidation.

Physisorption and pore size distribution measurements were carried out on a Micromeritics ASAP 2010C sorption analyzer. The passivated samples were degassed at 473 K under vacuum for 8 h prior to each measurement. The specific surface area S_g of the samples was determined by the N_2 BET method. The Barrett–Joyner–Halenda (BJH) numerical integration method (41) was used to measure mesopore distribution. The Horvath and Kawazoe equation was employed to determine the micropore distribution (42). The Halsey equation was used to calculate the adsorbed film thickness (43, 44).

Powder X-ray diffraction (XRD) measurements were conducted using a Mac Science M18XHF diffractometer with Cu Kα radiation. CS-444 carbon/sulfur analyzer (Leco) determined carbon and sulfur content of the catalysts after HDS reaction.

The morphology of those passivated samples was observed by scanning electron microscopy (SEM) on a Jeol JSM-840A. Electron probe microanalysis (EPMA) was employed on a Jeol JXA-8600 with wavelength-dispersive spectroscopy (WDS) to determine the lateral distribution of P and S, and energy-dispersive spectroscopy (EDS) was used to measure their concentrations. For these analyses, samples were mounted on graphite stubs, and gold was sputtered onto them to ensure an adequate conductivity. Electron microscopy was conducted using a Philips CM200 transmission electron microscope (TEM) with an operation voltage of 200 kV. The passivated samples were finely ground in a mortar to fine particles, ultrasonically dispersed in methanol, and then deposited on a Cu grid covered by a holey carbon film for measurements.

X-ray photoelectron spectroscopy (XPS) measurements were conducted using a Perkin-Elmer PHI 5400 ESCA spectrometer with monochromatic Mg Kα radiation (1253.6 eV) at 15 kV and 20 mA. About 0.2 g catalysts in a passivated form were pressed into a pellet at 34 MPa for XPS measurements. The spectrometer energies were calibrated using Au $4f_{1/2}$ peak at 84.0 eV, Ag $3d_{5/2}$ at 368.0 eV and Cu $2p_{3/2}$ at 932.6 eV as reference. Vacuum in the test chamber during the collection of spectra was maintained below 5×10^{-9} torr. Spectra were collected with analyzer pass energy of 89.450 eV for survey scan and 71.550 eV for multiple scans. In order to obtain reproducible results, a strict standardization of the order and the time of recording was used. The charging effect was circumvented by referencing the binding energies to that of C_{1s} peak of 285.0 eV. Overlapped peaks were deconvoluted by curve fitting using a nonlinear-least-squares algorithm (45). Depth profiles were obtained by bombardment of Ar^+ ion on the samples at a sputtering rate of 3 nm per minute for 10 cycles until 24 nm surface was removed.

RESULTS

Hydrodesulfurization of Benzothiophene

Shown in Fig. 1 are the reaction rates of the HDS of BTP as a function of temperature over Mo_2N prepared from different precursors. The reaction rate is expressed in the areal rate, i.e., the moles of BTP reacted per second per unit surface area of the catalyst measured before the reaction. The HPA-derived Mo_2N showed about 4 times higher reaction rates than those of Mo_2N prepared from $MoO_3 + P_2O_5$, and 5 to 7 times higher rates than those of P-free Mo_2N over the whole temperature range investigated. At temperatures lower than 673 K, the reaction rates increased with increasing the temperature. However, excessively high temperatures were detrimental to the HDS reaction for all the catalysts.

Unlike the hydrodenitrogenation of indole from which a variety of products were obtained, ethylbenzene was almost the exclusive product with toluene and benzene accounting for less than 1 wt% of the products in HDS of BTP.

The changes of reaction rates of HDS of BTP with time on stream at 573 and 673 K are given in Figs. 2 and 3. At 573 K, the reaction rates of HDS of BTP declined markedly with time on stream for HPA-derived Mo_2N, while the rates for Mo_2N prepared from $MoO_3 + P_2O_5$ and MoO_3 decreased much slower. Yet at 673 K, the HDS rates changed little during 6-h run for all three catalysts. In both cases, Mo_2N prepared from HPA showed the highest rate, while the other two gave similar rates with Mo_2N prepared from $MoO_3 + P_2O_5$ showing a little higher rate.

Encouraged by the above results that the rates of HDS of BTP over Mo_2N increased by adding P_2O_5 to the precursor MoO_3 and no evident deactivation was observed during 6-h run at 673 K, 120-h run was carried out to check their long-term performance of Mo_2N catalysts. The experimental conditions were identical to those mentioned above except that the flow rate of H_2 was reduced to 30 μmol s^{-1}. As shown in Fig. 4, the presence of phosphorus not only favored the HDS activity but also contributed to the resistance against catalyst deactivation. The initial rates of HDS of BTP over Mo_2N increased by more than 40% when adding P_2O_5 to the precursor MoO_3. However, the HDS rates decreased by only 10% after 120-h reaction for P-containing Mo_2N, while the HDS rates decreased by nearly 50% after 80-h run for P-free Mo_2N.

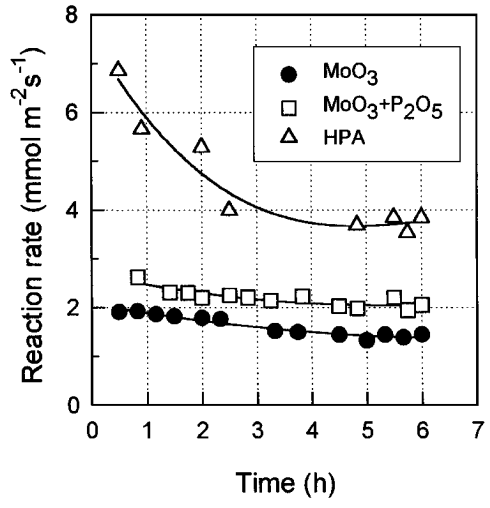

FIG. 2. Reaction rates of HDS of BTP with time on stream over Mo_2N prepared from different precursors: BTP feeding rate = 0.1 cm^3 h^{-1}; H_2 flow rate = 90 μmol s^{-1}; catalyst loading = 1.03 g; reaction temperature = 573 K.

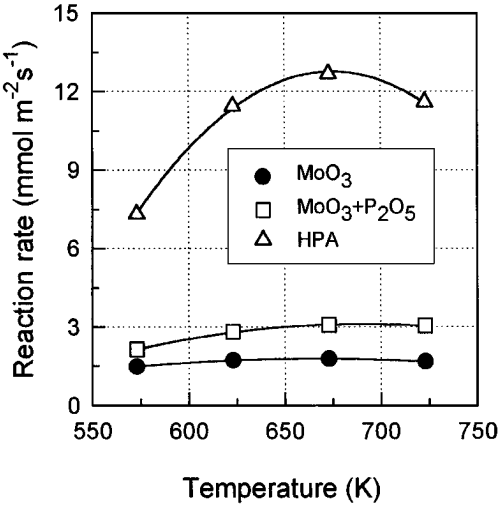

FIG. 1. Reaction rates of HDS of BTP as a function of temperature over Mo_2N prepared from different precursors: BTP feeding rate = 0.1 cm^3 h^{-1}; H_2 flow rate = 90 μmol s^{-1}; catalyst loading = 1.03 g.

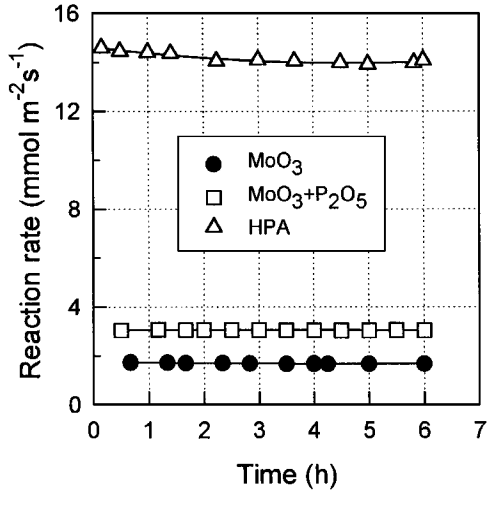

FIG. 3. Reaction rates of HDS of BTP with time on stream over Mo_2N prepared from different precursors: BTP feeding rate = 0.1 cm^3 h^{-1}; H_2 flow rate = 90 μmol s^{-1}; catalyst loading = 1.03 g; reaction temperature = 673 K.

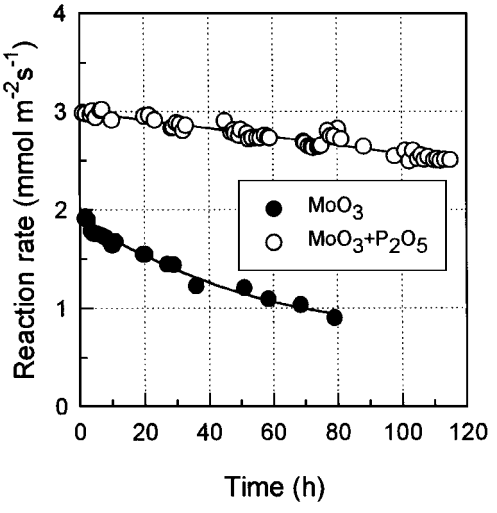

FIG. 4. Reaction rates of HDS of BTP with time on stream over Mo_2N prepared from MoO_3 and $MoO_3+P_2O_5$: BTP feeding rate = 0.1 cm^3 h^{-1}; H_2 flow rate = 30 μmol s^{-1}; catalyst loading = 1.03 g; reaction temperature = 673 K.

Adsorption and Pore Size Distribution

Figure 5 shows the N_2 adsorption and desorption isotherms at liquid nitrogen temperature for Mo_2N prepared from different precursors before (Fig. 5a) and after HDS of BTP at temperatures between 573 to 723 K (Fig. 5b). According to the classification of Brunauer (46), the isotherm of Mo_2N prepared from MoO_3 is the combination of type I and type IV, indicative of the presence of both micropores and mesopores. The addition of P_2O_5 causes reduction of adsorbed N_2 yet changes little the shape of the isotherm. However, the isotherm of Mo_2N prepared from HPA is quite different, suggesting Type II, which is commonly encountered on macroporous materials. In terms of de Boer classification (47) of the five types of hysteresis loop that represents the nature of the condensation process in the pores depending on the associated pore shapes, the hysteresis loops of Mo_2N prepared from MoO_3 and $MoO_3+P_2O_5$ are of type B, which is originated from slit-shaped pores or space between plates. Probably, the space between Mo_2N plates (Figs. 9 and 10) is responsible for the shape of the hysteresis. In the case of Mo_2N prepared from HPA, its isotherm exhibits only mild hysteresis and the shape does not belong to any of the five types. As shown in Fig. 5b, the amount of adsorbed volume decreases after HDS reaction for all the catalysts. However, the shape of isotherm changes little, suggesting that the adsorption behavior is rarely influenced by HDS reaction.

Pore size distribution are illustrated in Fig. 6 for these samples before (Fig. 6a) and after HDS of BTP (Fig. 6b) at temperatures between 573 to 723 K. For Mo_2N prepared from MoO_3 and $MoO_3+P_2O_5$, most of the pores are within a narrow distribution range between 2 to 4 nm with the

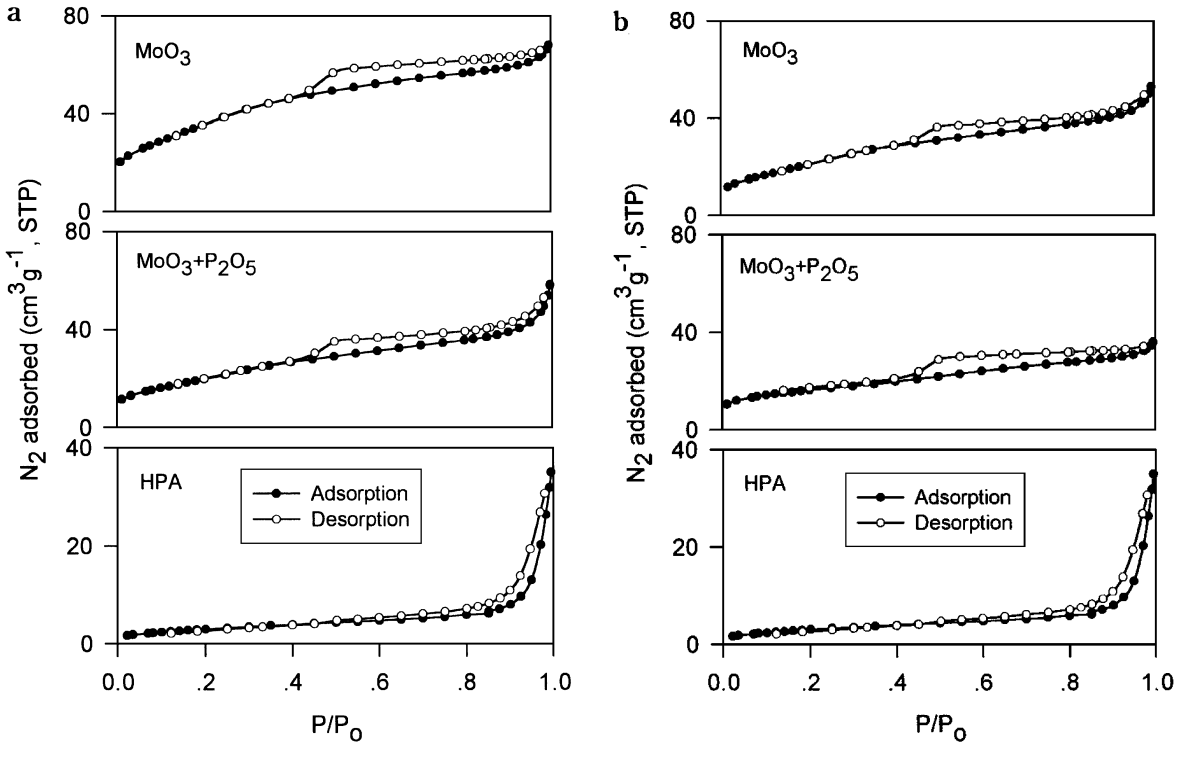

FIG. 5. Adsorption isotherm at LN_2 temperature for Mo_2N prepared from different precursors before reaction (a) and after HDS of BTP at temperatures between 573 to 723 K (b).

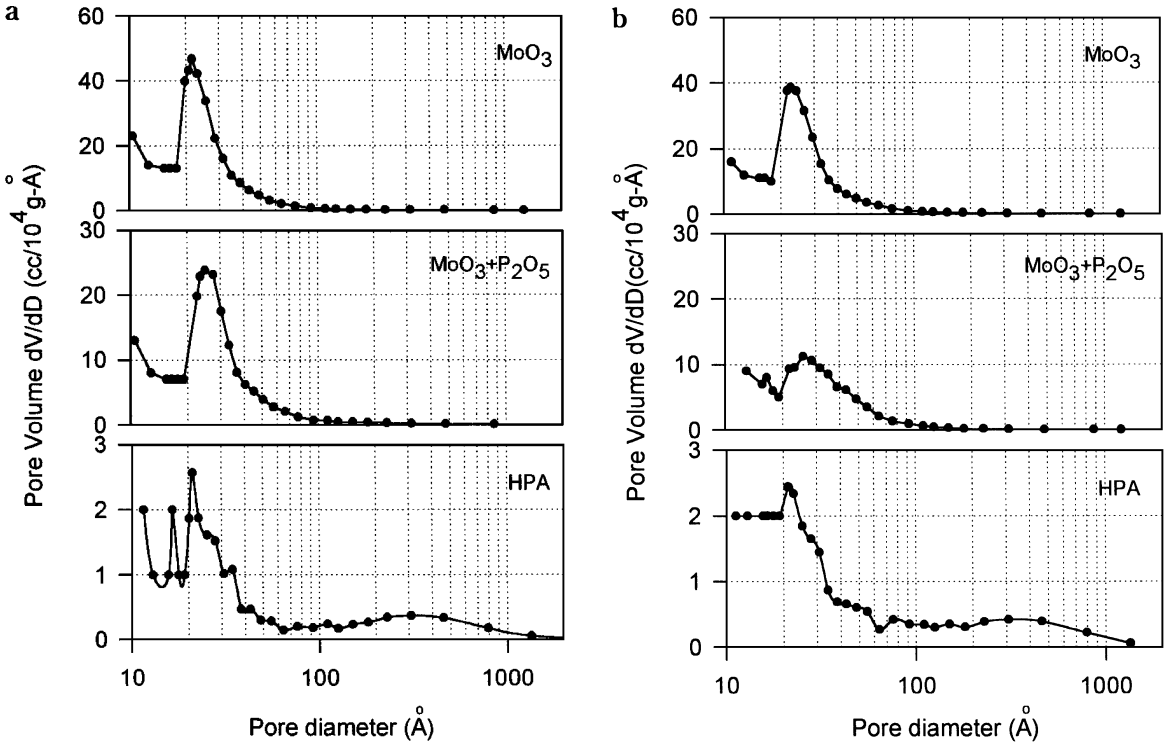

FIG. 6. Pore size distribution of Mo_2N prepared from different precursors before reaction (a) and after HDS of BTP at temperatures between 573 to 723 K (b).

latter showing a slightly larger average pore size. In the case of HPA-derived Mo_2N, the pores are irregularly distributed from micropores to mesopores. Also, there is a certain amount of macropores. The distribution of pore size for P-free Mo_2N changes only a little after HDS reaction over mesopore range. However, pore size distribution for Mo_2N prepared from $MoO_3 + P_2O_5$ is fairly broader at the mesopore range. In the case of HPA-derived Mo_2N, the pores are still distributed over a wide range from micropores to macropores after HDS reaction with minor change. However, this minor distribution change of pore size does not provide much information since the adsorption capacity is rather small for HPA-derived Mo_2N. The broad pore distribution and small adsorption capacity for HPA-derived Mo_2N appear to be responsible for its less characteristic hysteresis loop.

The volume of adsorbed N_2 versus the thickness of the adsorbed layer (V-t) provides us with the information about microporosity. The V-t curves of the fresh catalysts (Fig. 7a) indicate that a certain amount of micropores exists in all these catalysts regardless of precursors, while the amount of micropores decreases in the order of P-free Mo_2N, followed by Mo_2N prepared from $MoO_3 + P_2O_5$, and then HPA-derived Mo_2N. The slight but continuous bending of V-t curves implies a broad distribution of micropores in these samples. The V-t plots of the catalysts after HDS of BTP (Fig. 7b) display that the amount of micropores decreases appreciably for P-free Mo_2N, compared to P-containing samples.

The possibility of mass transfer limitation was tested by estimating the Weisz–Prater factor (48) which represents the ratio of reaction rate to the rate of pore diffusion of our reaction system. The values were in the range of 10^{-5}–10^{-6}, suggesting very little chance of diffusion limitation.

The surface areas and average pore sizes for Mo_2N prepared from different precursors are summarized in Table 1. These surface areas are smaller than those reported in the previous paper (39) since present results were obtained from passivated samples. However, the surface areas of

TABLE 1

Characteristics of Mo_2N Catalysts Prepared from Different Precursors for HDS of BTP

Precursor	MoO_3	$MoO_3 + P_2O_5$	HPA
Surface area/$m^2\ g^{-1}$			
Before reaction	118.5	72.7	14.2
After reaction[a]	78.2	56.0	11.1
Average pore diameter[b]/Å			
Before reaction	31.7	38.9	118.8
After reaction	34.9	42.2	116.5

[a] After HDS of BTP at different temperatures between 573 to 723 K.
[b] Determined from pore size distribution, measured by N_2 adsorption.

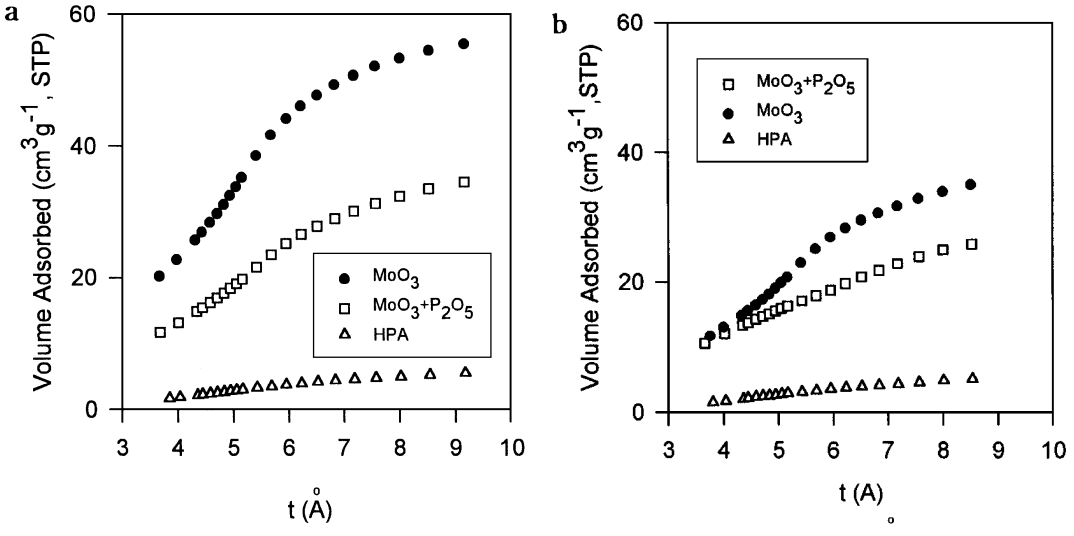

FIG. 7. V-t plot of Mo_2N prepared from different precursors before reaction (a) and after HDS of BTP at temperatures between 573 to 723 K (b).

all the catalysts show the same trend with P-free Mo_2N having the highest surface area followed by Mo_2N prepared from $MoO_3 + P_2O_5$, and then HPA-derived Mo_2N, which has surface area of only 14.2 $m^2\ g^{-1}$. After HDS of BTP, the surface areas decrease greatly for all the catalysts.

The average pore diameter of Mo_2N prepared from MoO_3 increases by adding P_2O_5 to the precursor MoO_3. Moreover, both average pore diameters increase after HDS of BTP, suggesting the blocking of small pores. In the case of HPA-derived Mo_2N, the extremely large average pore diameter of HPA-derived Mo_2N is due to the wide range of pore size distribution of its mesopores and macropores. The slight change in average pore diameter after HDS of BTP should be taken as within the error range.

Blocking of smaller pores seems responsible for the decreased surface area and the apparently increased pore size of Mo_2N due to the addition of P_2O_5 (39). Yet another factor must account for the further decrease of surface area and the increase of average pore size for all these samples after HDS reaction. Together with the observed change in pore size distribution (Fig. 6) and V-t curves (Fig. 7) after the reaction, we can conclude that smaller pores in these catalysts are blocked during the reaction as well.

Bulk Structure and Morphology

X-ray diffraction patterns for Mo_2N prepared from different precursors after HDS of BTP at temperatures between 573 and 723 K are shown in Fig. 8. Compared to the XRD patterns of fresh samples reported in the previous paper (39), no noticeable change was observed. Similar XRD patterns were obtained for the samples after HDS of BTP under the other conditions and, thus, are not provided here.

The morphologies shown in SEM micrographs and EPMA-WDS of sulfur and phosphorus after HDS of BTP at temperatures between 573 and 723 K are given in Fig. 9 for Mo_2N prepared from precursor MoO_3, Fig. 10 for Mo_2N from $MoO_3 + P_2O_5$, and Fig. 11 for Mo_2N from HPA. The morphologies appear unaltered when compared to those SEM images of the fresh sample (39). By means of EPMA, a significant amount of sulfur was observed present in the after-run catalysts regardless of the precursors, and sulfur was so heavily deposited on the surface that its signal was much stronger than that of phosphorus in P-containing catalysts. Since the EPMA measurements were performed under the identical condition, the stronger sulfur signal on P-free Mo_2N sample indicates that there are more sulfur

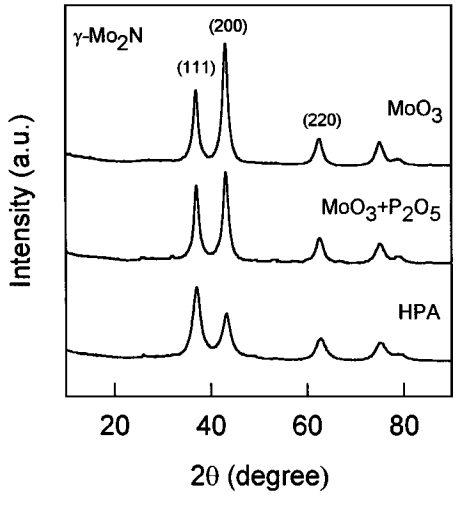

FIG. 8. X-ray diffraction patterns of Mo_2N prepared from different precursors after HDS of BTP at temperatures between 573 to 723 K.

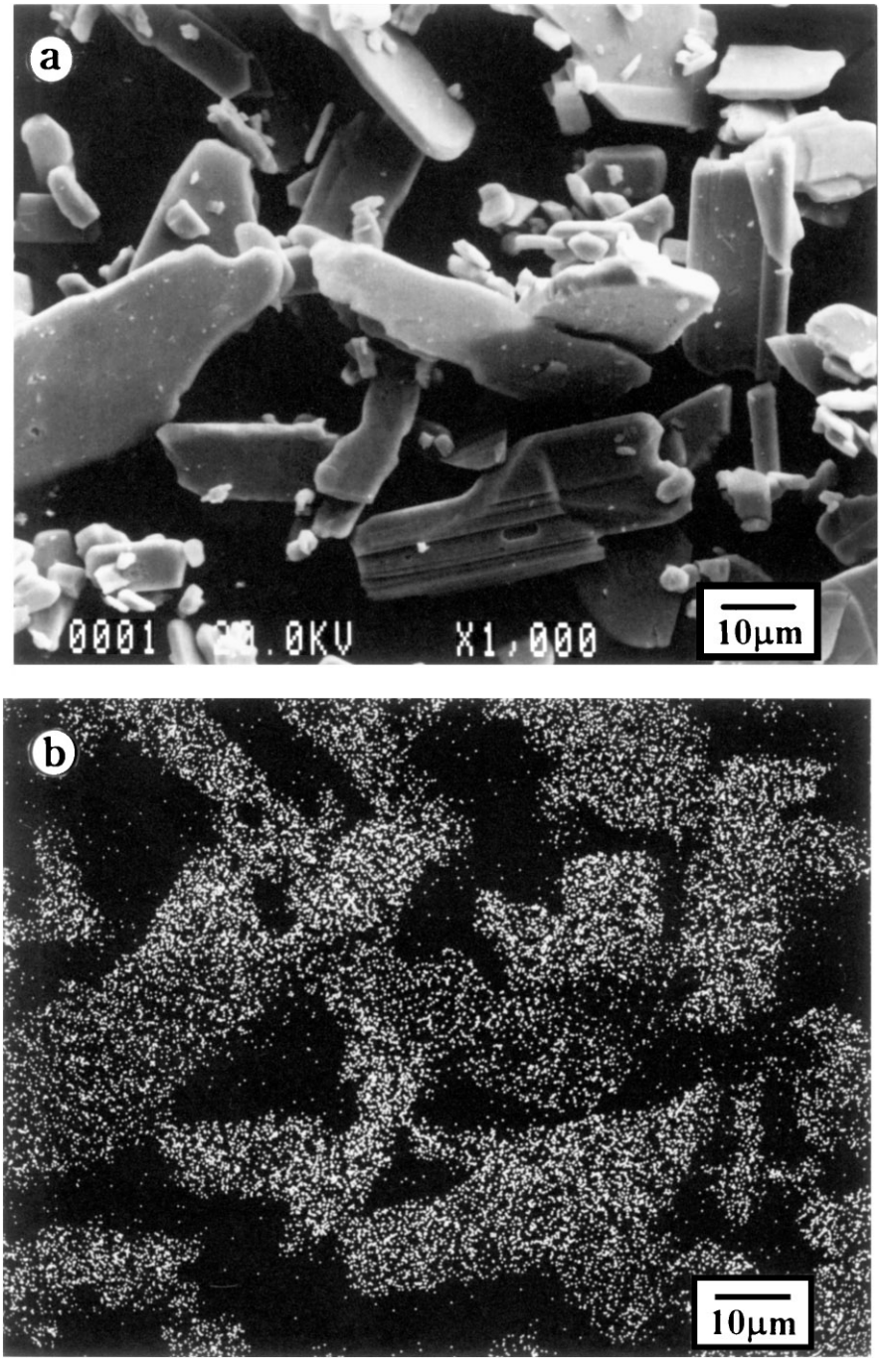

FIG. 9. Scanning electron micrograph (a) and EPMA of sulfur (b) of Mo_2N prepared from MoO_3 after HDS of BTP at temperatures between 573 to 723 K.

compounds deposited on this catalyst. This fact was confirmed by quantitative analysis of chemical analysis, EDS, and XPS as described below. The morphology and EPMA of the three Mo_2N samples after HDS at 673 K for 6 h provide the qualitatively identical information, and thereby are not given here.

XPS Results

Figure 12 shows the XPS depth profiles of Mo_2N catalysts after HDS of BTP at 673 K for 6 h. The S_{2p} peaks with a binding energy at 168.2 ± 0.2 eV, representing a sulfate form (49), is observed on the outmost surface of the

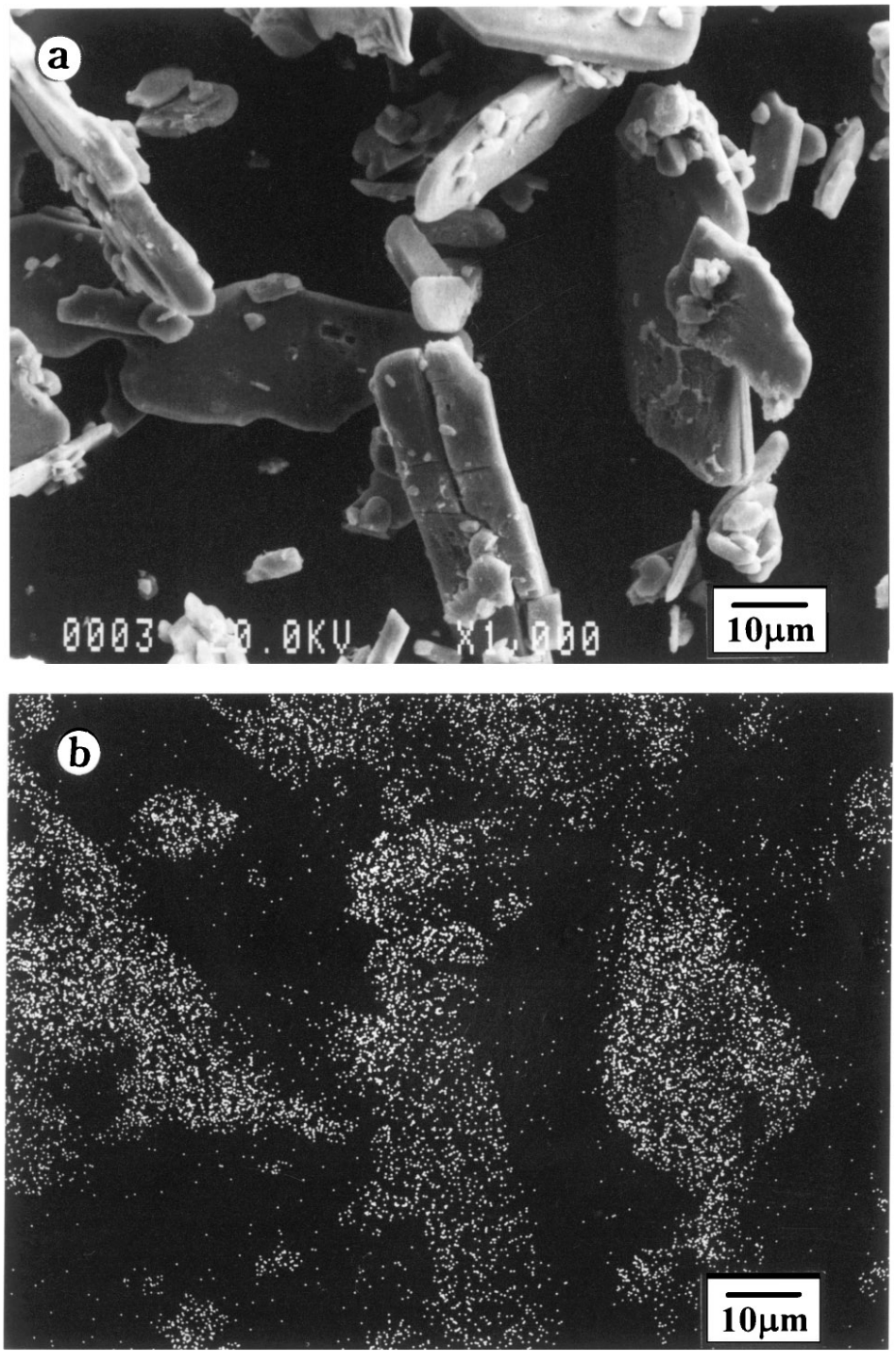

FIG. 10. Scanning electron micrograph (a) and EPMA of sulfur (b) and phosphorus (c) of Mo_2N prepared from $MoO_3 + P_2O_5$ after HDS of BTP at temperatures between 573 to 723 K.

catalysts. However, the binding energy of S_{2p} peak moves to 162.1 ± 0.2 eV, which could be assigned to a sulfide form (49), after sputtering away the surface of 3 nm. The assignment of S_{2p} binding energy at 162.1 ± 0.2 eV to S^{2-} is in accord with the value proposed by Alstrup and Brown (50, 51). The surface sulfate at 168.2 eV probably results from the oxidation of S^{2-} to SO_4^{2-} due to exposure of the catalysts to air. Similar observation has been reported by Woo *et al.* (52) on MoS_2 slabs. It has also been reported that MoS_2 has a S_{2p} binding energy of 162.5 eV (53). In industrial

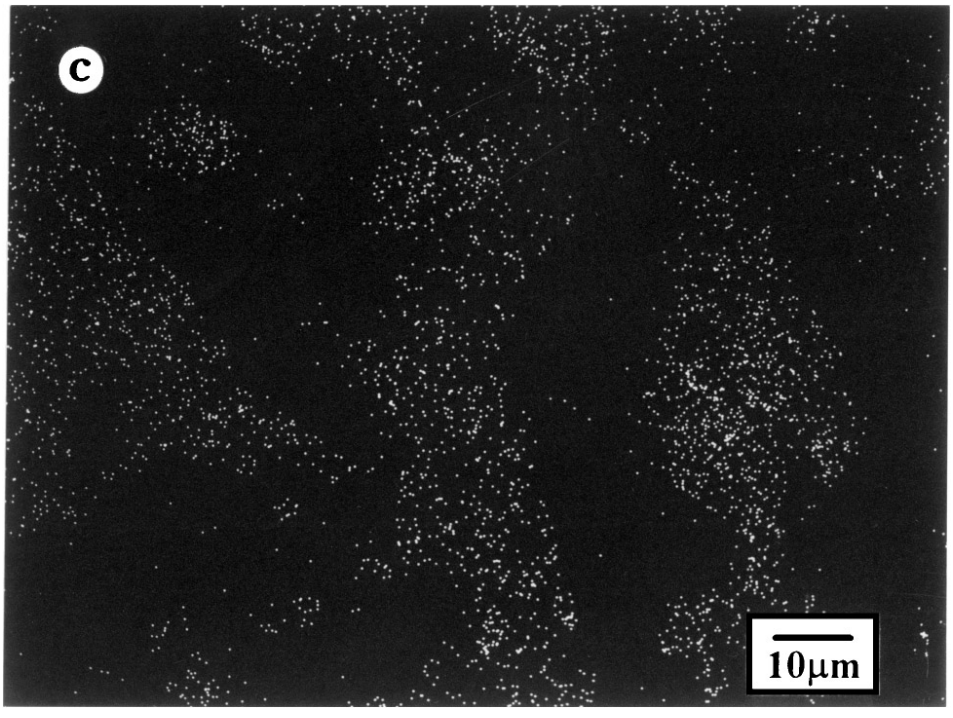

FIG. 10—*Continued*

process MoO_3 is sulfided under H_2S/H_2 flow at 673 K which is within the temperature range of HDS reaction. In our study, H_2S formed as a product of hydrodesulfurization. Therefore, it is plausible to assume that parts of the catalysts could be sulfided *in-situ* during the HDS reaction to form molybdenum sulfide.

The profile of P_{2p} level along the depth of surface shows a main peak with binding energy at 133.8 ± 0.2 eV, which corresponds to that of a phosphate form. There is also a small peak with binding energy at 129.7 ± 0.2 eV under the surface, suggesting the coexistence of phosphide form (40). The resembling S_{2p} peaks regardless of the precursors suggest that the addition of phosphorus does not change the chemical state of Mo–S bonds. Yet, it is likely to influence the amount of sulfur deposits.

The N_{1s} peak is overlapped with that of Mo_{2p}. The deconvolution gives a peak with binding energy centered at 397.0 ± 0.2 eV, which corresponds to a nitride form (49). This assignment verifies the association of nitrogen with molybdenum.

Mo_{3d} gives triplet peaks with binding energy centered at 228.8, 232.2, and 235.8 ± 0.2 eV, respectively, implying the coexistence of various Mo species such as nitride, sulfide, and oxide forms. Two envelopes centered at 232.2 and 235.8 eV represent the characteristic doublet Mo_{3d} of Mo^{6+}. Here, we ascribe the Mo peak with binding energy at 228.8 ± 0.2 eV to Mo associated with nitrogen based on the following considerations. First, substantial amounts of nitrogen, which exist in a nitride form, necessitate the presence Mo–N bonding. Second, the peak position is the same as that we found for Mo_2N used for HDN of indole where there is no sulfur present in the system (40). Finally, the binding energy of Mo–N must be lower than that of Mo–S from MoS_2. Patterson proposed 229.0 eV and Grim reported 229.6 eV as the binding energy of Mo in MoS_2 (54, 55). The Mo_{3d} peaks due to the sulfide in Mo_2N catalysts appeared to be masked by other dominant species.

The peak area of the species along the depth of the surface for Mo_2N prepared from MoO_3, $MoO_3 + P_2O_5$, and HPA after HDS reaction are shown in Figs. 13a, 13b, 13c, respectively. Along the depth of the catalyst surface into the bulk, the amount of nitrogen increases while that of molybdenum decreases gradually, approaching the stoichiometry of Mo_2N. More sulfur compounds are found deposited on the P-free sample and its amount decreases along the depth of the surface. In P-containing catalysts, both amounts of phosphorus and sulfur decrease along the depth of the surface, indicating the segregation of phosphorus from the bulk to the surface and the diffusion of sulfur from the surface into the lattice.

Quantitative Analysis of Sulfur and Phosphorus

The quantitative analysis of sulfur and phosphorus after HDS of BTP at 673 K for 6 h were performed via C/S analyzer, EDS, and XPS. The results summarized in Table 2 provide us with the information along the surface to

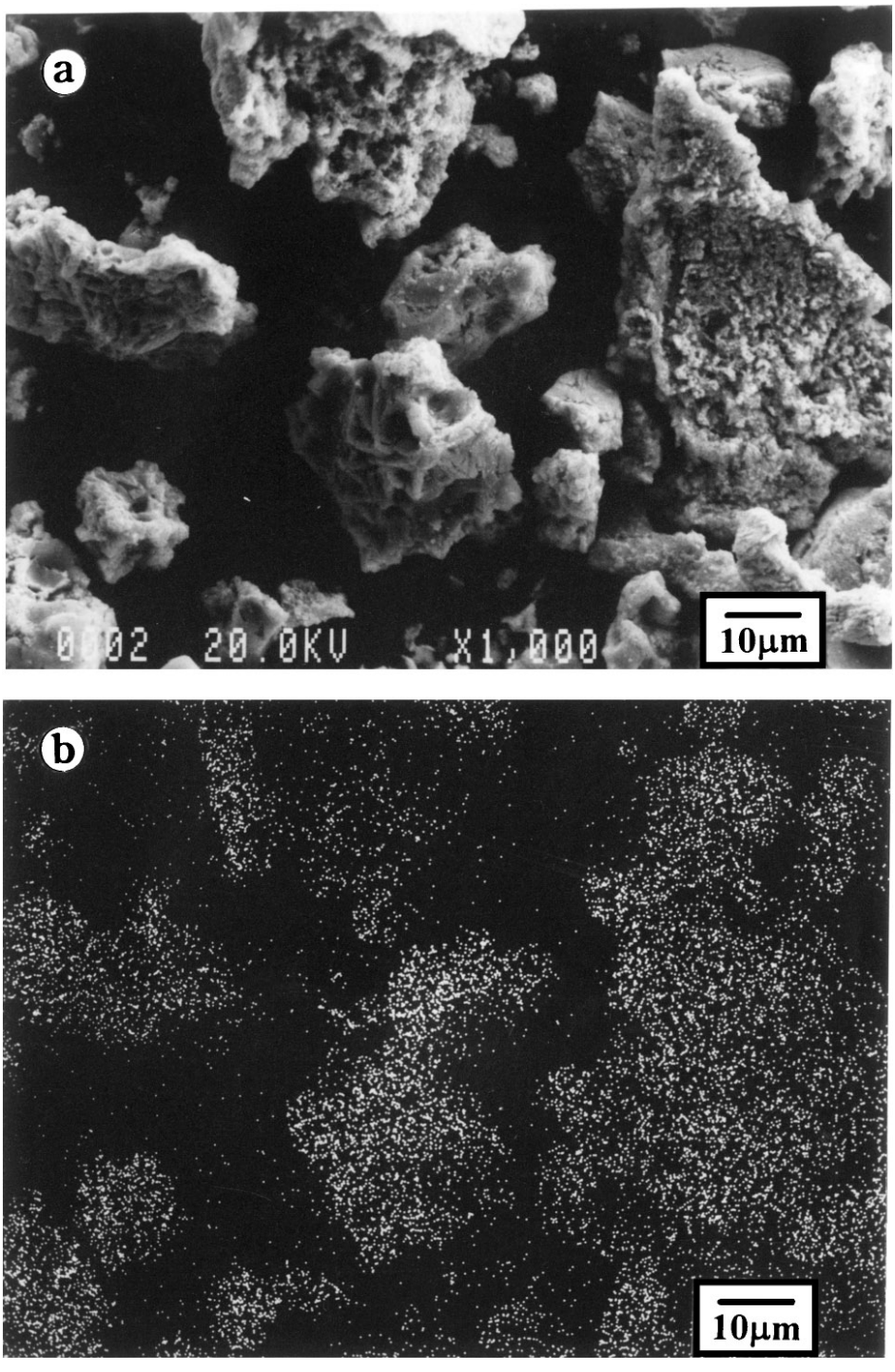

FIG. 11. Scanning electron micrograph (a) and EPMA of sulfur (b) and phosphorus (c) of Mo_2N prepared from HPA after HDS of BTP at temperatures between 573 to 723 K.

the bulk. These measurements show a consistent tendency that P-free Mo_2N contained the largest amount of sulfur, not only on the surface but also in the bulk, followed by Mo_2N prepared from $MoO_3 + P_2O_5$, and then least amount of sulfur is present in HPA-derived Mo_2N catalyst. More phosphorus is present on the surface of Mo_2N prepared from $MoO_3 + P_2O_5$, which is in accord with our previous observation in HDN of indole (40). However, there is no significant difference among catalysts in their carbon contents.

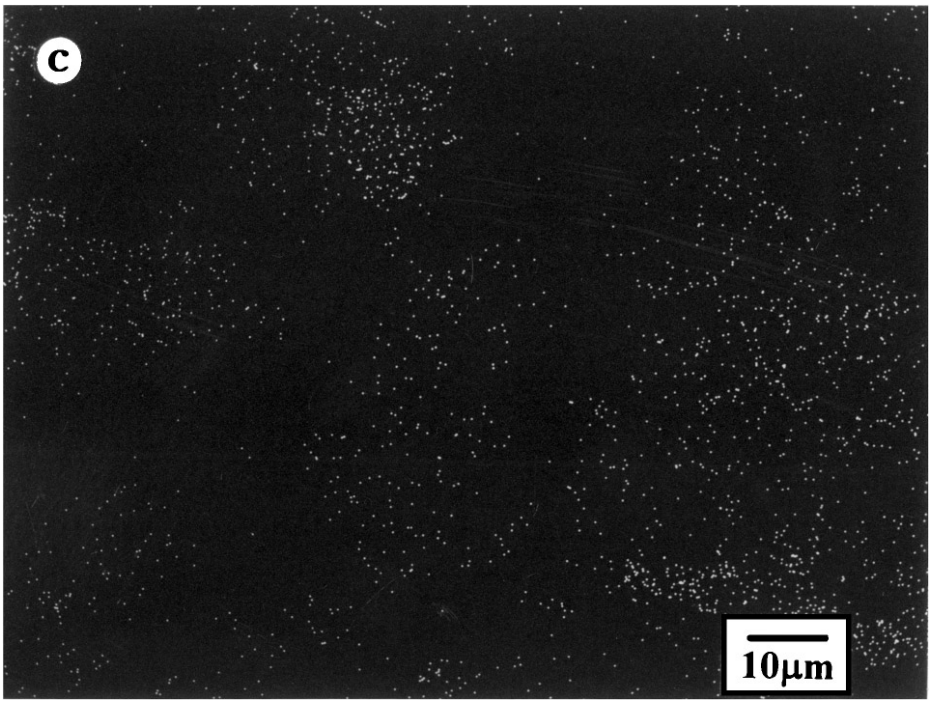

FIG. 11—*Continued*

TEM Observation

Mo_2N prepared from MoO_3, $MoO_3 + P_2O_5$, and HPA before and after HDS reaction at temperatures between 573 and 723 K were investigated by transmission electron microscope (TEM). The bright field (BF) image of a small aggregate and the corresponding selected-area diffraction (SAD) patterns are given in Figs. 14, 15, and 16.

The bright-field images of these samples (Figs. 14a and b, 15a and b, 16a and b) show the randomly distributed small domains, representing the particles that comprised the Mo_2N platelet. This type of image contrast is caused by density variation in the specimen and is commonly encountered in porous solids. No significant difference in BF images was observed between the samples before and after HDS reaction. The average size of domains on TEM appears to be ca 4–6 nm and pore size of 2–4 nm. It is less tenable to determine the crystallite size and pore size by the BF image since the crystallites are so fine that some other factors such as thickness of the samples will influence the contrast. However, these values are within the same order as those results we obtained from XRD measurement for particle size (39) and from adsorption isotherms for pore size.

The electron diffraction pattern (Fig. 14c) of P-free Mo_2N shows clear spots with a square symmetry, indicative of the diffraction of (200) plane of well-defined crystallites of Mo_2N with face-centered-cubic structure. The topotactic relationship between MoO_3 and Mo_2N dictates that individual Mo_2N crystallites comprising the aggregate maintain the same crystallographic relationship as in the starting MoO_3 (56). Although a crystal of MoO_3 is broken into many 4–6-nm crystallites of Mo_2N during the MoO_3-to-Mo_2N transformation, these crystallites form an aggregate in which the position of a Mo atom in a crystallite is relative to other Mo atoms, and even to those in other crystallites, as far as the crystallites remained in the same aggregates. However, rather than a perfect crystal, the appearance of diffuse rings in the background reveals that there are misorientation between crystal planes. This observation is in good agreement with that of Volpe and Boudart (27). The enhanced intensity of rings on Mo_2N after reaction demonstrates that the crystallographic misorientation or polycrystallinity has become severer after HDS reaction (Fig. 14d).

TABLE 2

Quantitative Analysis of Sulfur and Phosphorus for Mo_2N Catalysts after HDS of Benzothiophene at 673 K for 6 h

	Chemical analysis[a] (wt %)		EDS (atom %)		XPS (atom %)	
Precursor	C	S	S	P	S	P
MoO_3	0.82	4.77	5.80	—	4.42	—
$MoO_3 + P_2O_5$	0.88	3.70	4.00	3.01	2.82	1.81
HPA	0.72	1.95	4.00	1.15	2.43	0.99

[a] Determined by C/S analyzer.

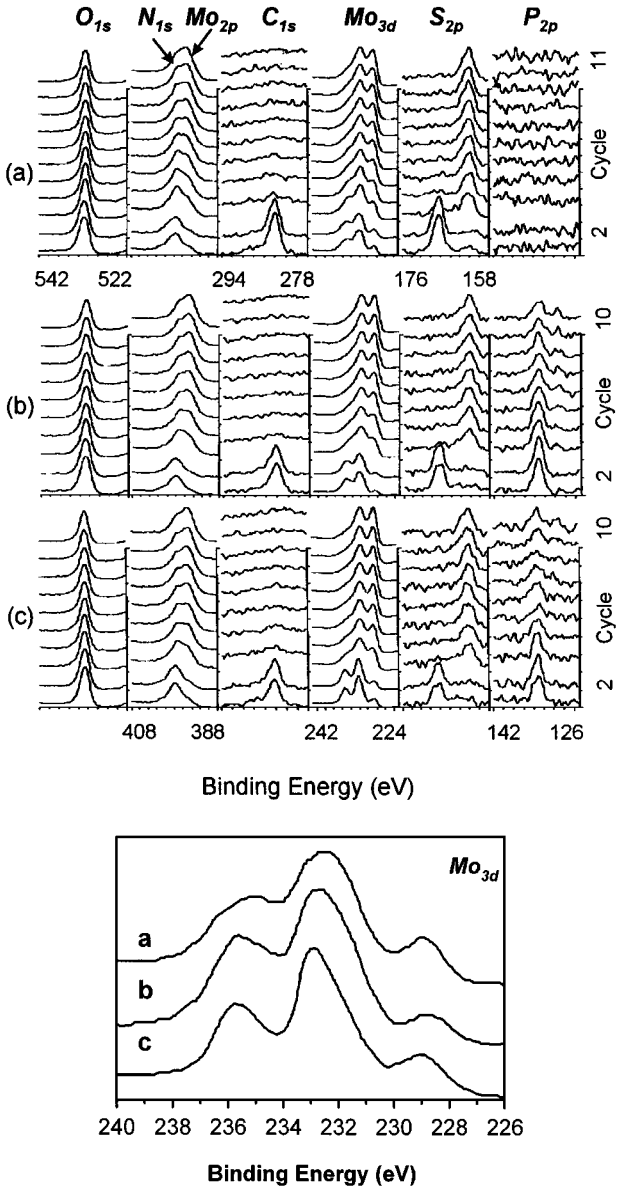

FIG. 12. Depth profiles of XPS analysis for Mo_2N prepared from different precursors after HDS of BTP at 673 K for 6 h: (a) Mo_2N prepared from MoO_3; (b) Mo_2N prepared from $MoO_3 + P_2O_5$; (c) Mo_2N prepared from HPA. Enlargement of Mo_{3d} region is shown in the bottom for three Mo_2N samples.

The SAD pattern of Mo_2N prepared from $MoO_3 + P_2O_5$ is given in Fig. 15c. The Mo_2N (fcc) phase is identified by its distinct (200) diffraction spots. Compared with P-free Mo_2N, clearer rings appear, indicating that polycrystallinity grows due to adding P_2O_5 to the precursor. Moreover, a new ring band, suggesting the presence of amorphous materials which most probably come from P_2O_5, is also observed. The polycrystallinity and amorphism get even more severe after the HDS reaction such that the diffraction spots are almost overshadowed (Fig. 15d). Similar behaviors were observed over P-containing HPA-derived Mo_2N (Fig. 16c and 16d).

As shown in XPS depth profiles, sulfur is able to diffuse into catalyst bulk to 20 nm that is far beyond the range of individual crystallite size. This suggests that sulfur goes into the catalysts and intervenes in the well-ordered Mo_2N lattice by bonding with Mo, resulting in crystalline misorientation; yet this interference appears to be limited to a small extent and not serious enough to change the XRD patterns.

DISCUSSION

Beneficial Effects of Phosphorus and Catalyst Deactivation in Hydrodesulfurization of Benzothiophene

On the basis of areal rates in HDS of BTP as reported in Figs. 1–4, P-containing Mo_2N, especially HPA-derived Mo_2N, showed higher reaction rates than that without phosphorus. As mentioned above, the reaction rates are based on the surface area of fresh catalysts. When the rates based on catalyst weight are compared, Mo_2N without phosphorus shows the highest rate, and P-containing Mo_2N catalysts register similar rates. If the rates are based on the amount of irreversible CO chemisorption for the fresh catalysts, the order of activity is the same as in Fig. 1. However, the difference among catalysts are much greater since the CO site densities (10^{14} cm^{-2}) for P-free Mo_2N, Mo_2N from $MoO_3 + P_2O_5$, and HPA-derived Mo_2N are 1.56, 0.25, and 0.09, as reported previously (39). In any case, the beneficial effect of phosphorus on the enhanced rates of HDS over Mo_2N is evident.

When P-free Mo_2N and Mo_2N prepared from $MoO_3 + P_2O_5$ are compared, P-containing catalysts were more resistant to deactivation. This behavior was quite distinct from that in HDN of indole, where P-containing catalysts improved the activity but was more vulnerable to deactivation. This improved stability due to phosphorus is not obvious for Mo_2N prepared from HPA as shown in Figs. 2 and 3. However, the amount of sulfur deposits in this catalyst during the reaction was similar to that for Mo_2N prepared from $MoO_3 + P_2O_5$ and much less than that for P-free Mo_2N. Since the catalyst derived from HPA is so much different from the other two Mo_2N catalysts in many physical properties (39, 40), the comparison of those two catalysts should be more meaningful in isolating the effect of phosphorus on the catalyst stability.

A consistent tendency has been found in XPS, EDS study, and element chemical analyses that P-free Mo_2N contains the highest amount of sulfur (Table 2). This trend is consistent with the ease of catalyst deactivation. Thus, the most plausible reason for the deactivation of catalysts is believed to be the deposition of sulfur compounds on the catalyst surface. As in the case of HDN of indole (40), there is no distinct difference among catalysts in their carbon contents. Moreover, the contents of carbon are much lower than that

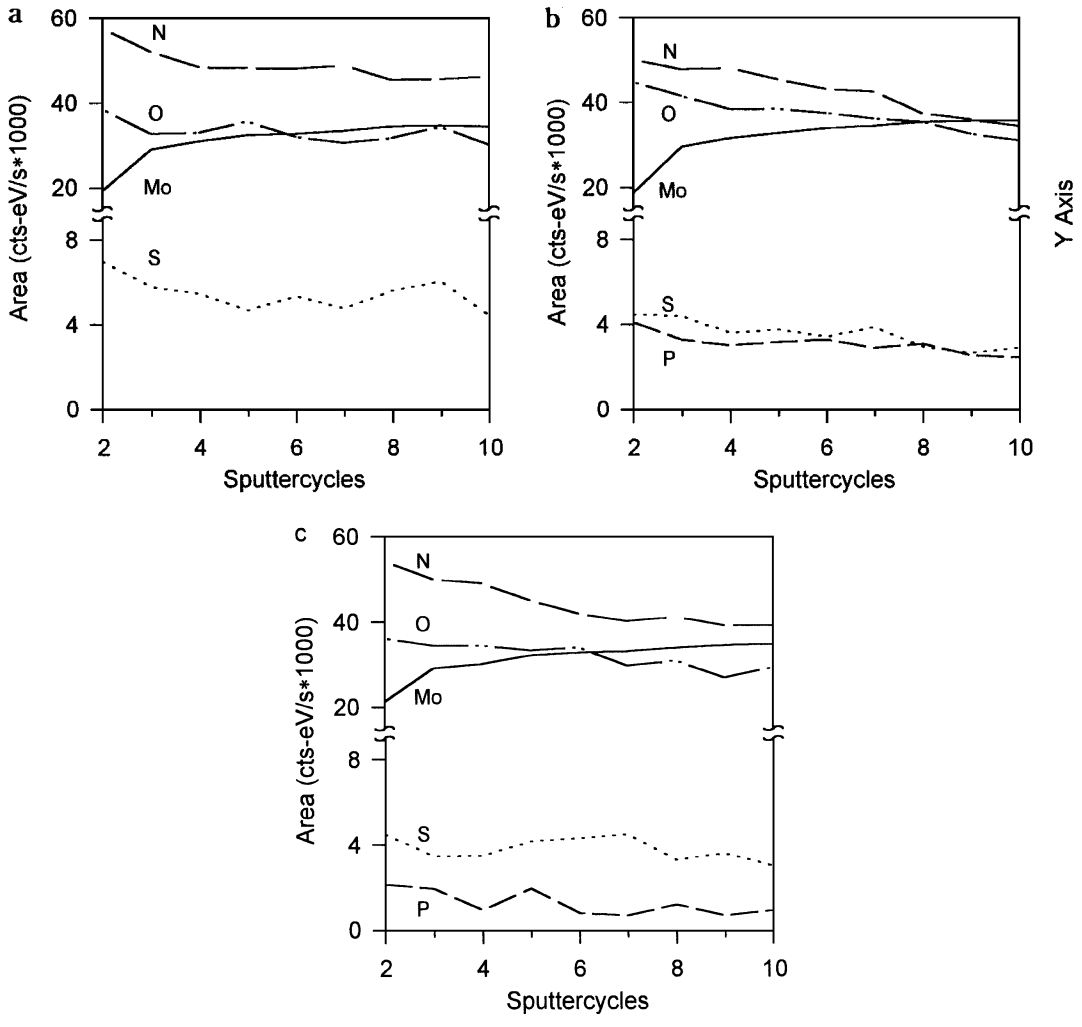

FIG. 13. Peak area of the elements along the depth of surface over Mo_2N prepared from MoO_3 after HDS of BTP at 673 K for 6 h (a); prepared from $MoO_3 + P_2O_5$ after HDS of BTP at 673 K for 6 h (b); prepared from HPA after HDS of BTP at 673 K for 6 h (c).

of sulfur. Therefore, carbon deposition does not account for the different behaviors of the catalysts in their resistance to deactivation.

As indicated by XPS analysis, sulfur is associated with Mo mostly as a sulfide. In Co(Ni)–Mo/γ-Al_2O_3, an industrial HDS catalysts, MoS_2 is commonly accepted as an active phase. However, this does not mean that all forms of MoS_2 contribute to the catalytic activity. It has been reported that only the less saturated edges on its characteristic slabs are believed to be active sites for HDS (4, 57). In our Mo_2N catalysts, sulfur compounds were deposited on the surface of the catalyst in such a manner that it acts as a poison that is responsible for the blocking of pores and the decreased surface area (Table 1). It is also likely that the sulfidation of the surface cause the particle/crystallite expansion, leading to further close-off of the pores. Anyway, it is sulfur compounds that account for the plugging of the smaller pores, and thus the deactivation of the catalysts. In P-free Mo_2N catalysts, more sulfur compounds were deposited on the surface, and consequently more micropores were blocked (Fig. 7b). Somorjai *et al.* (58, 59) carried out thiophene hydrodesulfurization over initially clean sulfided Mo (100) surface. It was observed that excessive exposure of the surface to a sulfur-containing environment resulted in the formation of a MoS_2 layer which was, at least in part, responsible for complete catalytic deactivation.

Accordingly, sulfur compounds deposited on the surface block the pores and thus account for the deactivation of Mo_2N catalysts. However, phosphorus, which is well distributed in a phosphate form, seems responsible for lowering sulfur deposits, and thus contributes to its improved resistance against deactivation.

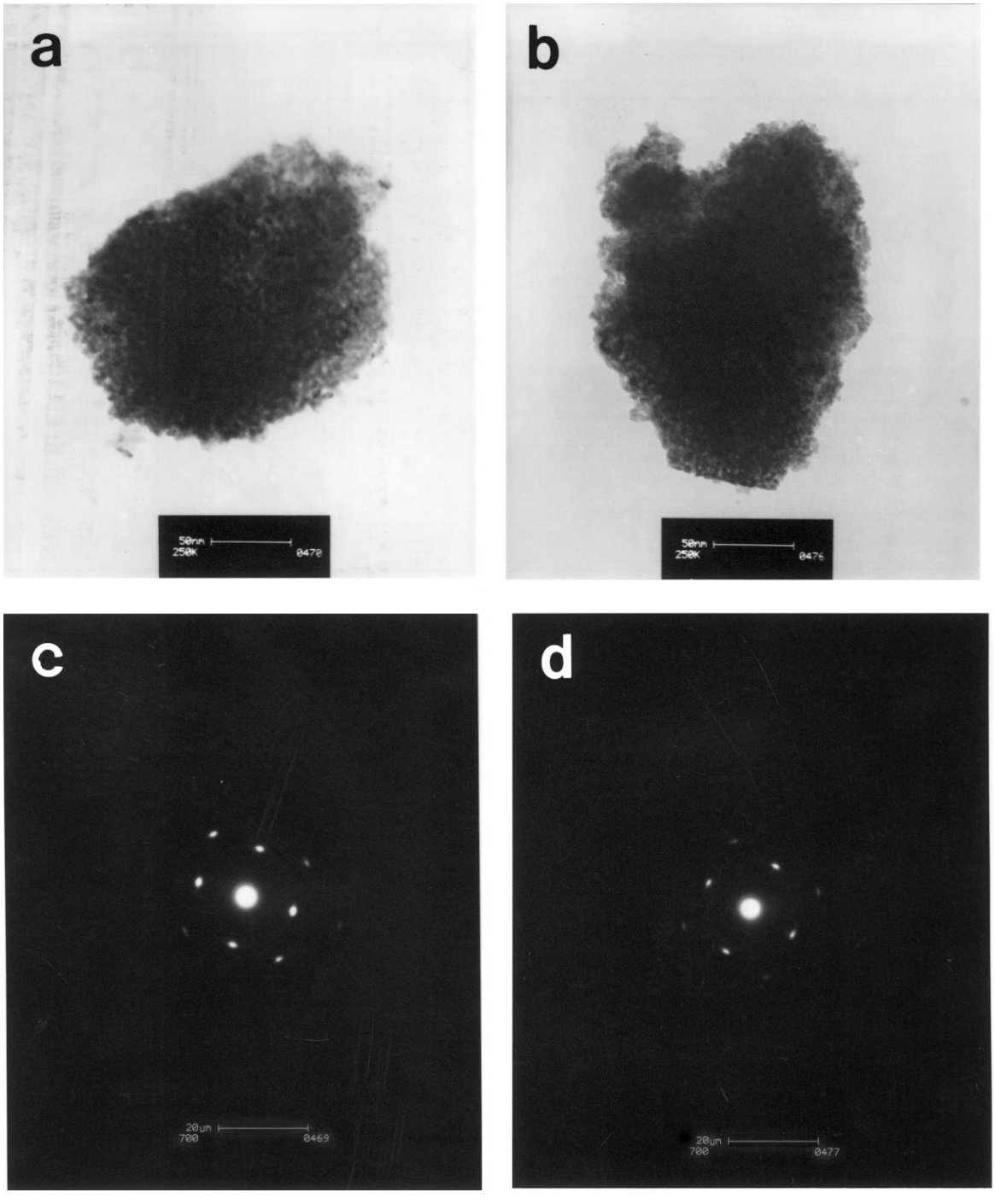

FIG. 14. Bright field images of TEM for Mo_2N prepared from MoO_3 (a) before and (b) after HDS reaction and its corresponding elected area diffraction patterns (c) before and (d) after HDS of BTP at temperatures between 573 to 723 K. The scales shown in the images denote 50 nm for (a) and (b), and 20 nm for (c) and (d).

Reaction Pathway of HDS of Benzothiophene and HDN of Indole

As proposed in the previous paper, HDN of indole involved three steps: hydrogenation of heteroatom-containing ring to indoline which is readily equilibrated, cleavage of C–N bond to ethylaniline, and then simultaneous hydrogenolysis of C–C and C–N bonds of ethylaniline. As a result the reaction product is a mixture of aniline and aromatic group compounds.

Both benzothiophene and indole are heterocyclic compounds of similar chemical structure. Thereby similar

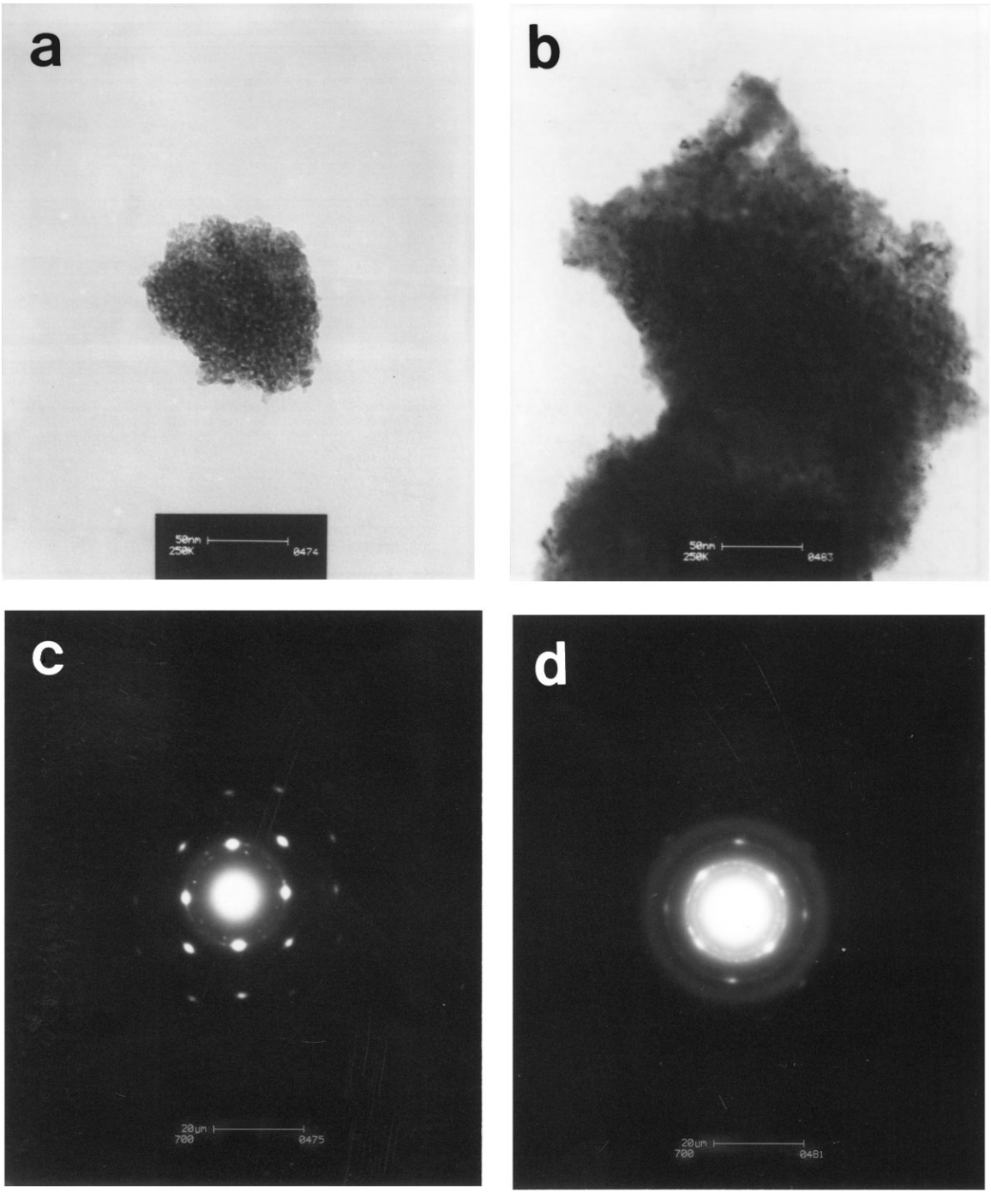

FIG. 15. Bright field images of TEM for Mo_2N prepared from $MoO_3 + P_2O_5$ (a) before and (b) after HDS reaction and its corresponding elected area diffraction patterns (c) before and (d) after HDS of BTP at temperatures between 573 to 723 K. The scales shown in the images denote 50 nm for (a) and (b), and 20 nm for (c) and (d).

reaction pathway and product distributions are anticipated. However, ethylbenzene is the overwhelming product in HDS reaction over the whole temperature range investigated. A small amount of ethylthiopenol was observed at lower temperatures, implying that it proceeds through the same route from equilibrated hydrogenation of BTP to tetrahydrobenzothiophene followed by the cleavage of C–S bond in the saturated ring to ethylthiopenol. The discrepancy of product distribution begins from the step of hydrogenolysis of ethylthiopenol. It is well known that an

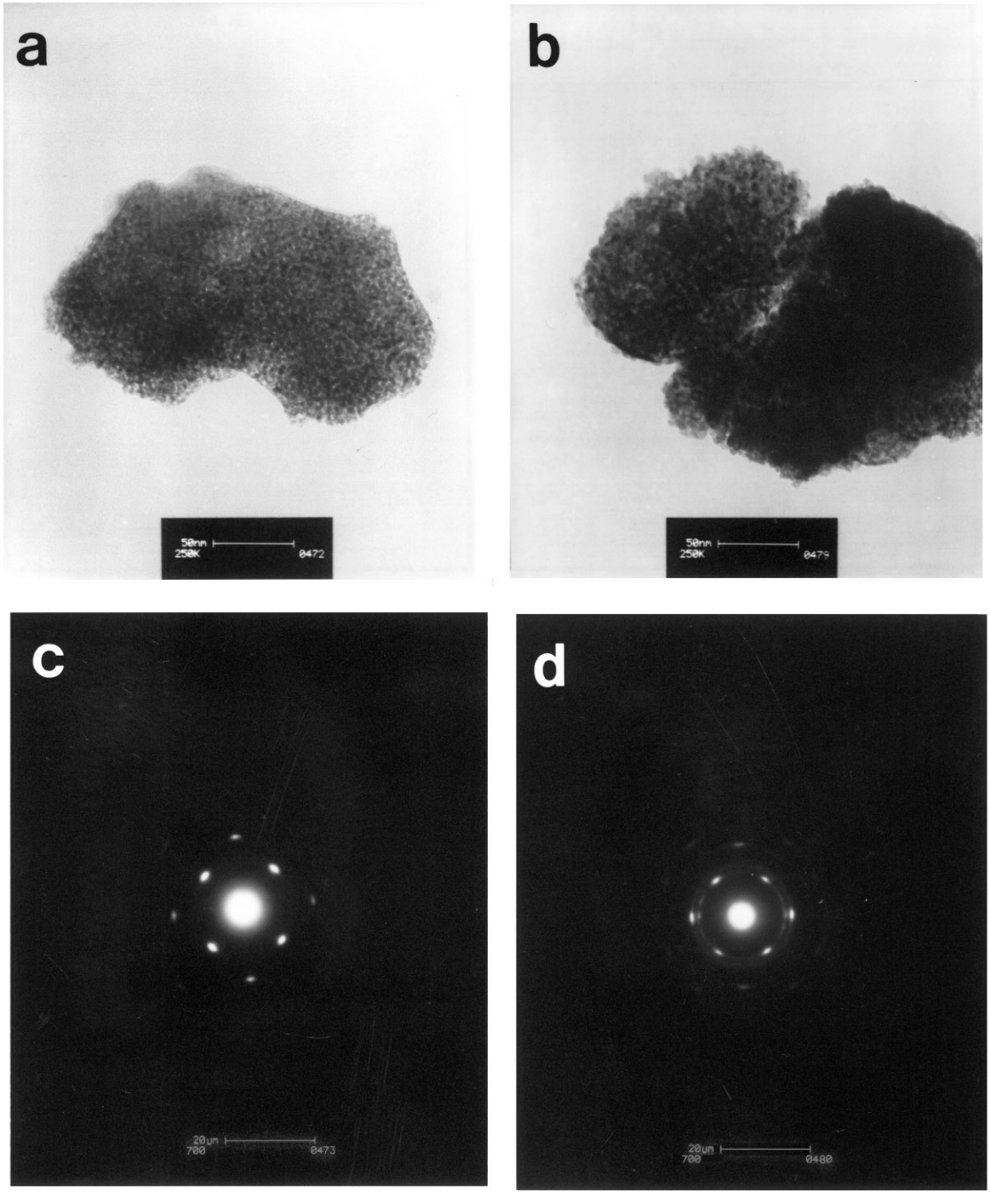

FIG. 16. Bright field images of TEM for Mo_2N prepared from HPA (a) before and (b) after HDS reaction and its corresponding elected area diffraction patterns (c) before and (d) after HDS of BTP at temperatures between 573 to 723 K. The scales shown in the images denote 50 nm for (a) and (b), and 20 nm for (c) and (d).

aromatic ring with electron-donating substitute such as NH_2, capable of stabilizing the carbocation intermediates, is more reactive toward electrophilic alkylation. The same rule must work in the dealkylation of substituted aromatic ring since it is just the reverse reaction of alkylation. Compared to SH, NH_2 is a much stronger activating functional group to the benzene ring. Thus, aniline and methlyaniline that result from dealkylation and hydrogenolysis of C–C bonds, are both present in HDN reaction, whereas ethlythiopenol is the only intermediate in HDS reaction. In

addition, since the atomic radius of S is much larger than that of C, hydrogenolysis of C–S bond will be much easier than that of C–N bonds that has stronger bonding. Consequently, hydrogenolysis of C–S bond of ethylthiophene, leading to ethylbenzene, will take priority over hydrogenolysis of C–C bond or dealkylation.

Comparison of HDS and HDN Reaction

Compared to the catalytic performance of Mo_2N in HDN of indole with that in HDS of BTP, Mo_2N is more active for HDS reaction. The addition of phosphorus to the precursor MoO_3 favors both reactions but with a different tendency. In HDN reaction, the addition of phosphorus increases the initial activity. However, the catalysts deactivate more readily with time on stream. On the contrary, in HDS reaction, phosphorus contributes to both improved reaction rates and resistance against deactivation.

According to the literature, phosphorus acts as a severe poison on carbon-supported molybdenum sulfide catalysts (60), whereas it served as a promoter for alumina-supported catalysts (61) in the hydrotreating process. It has been also reported that an appropriate amount of phosphorus added to the catalysts favors both HDN and HDS reactions. Yet an excessive amount of phosphorus adversely affects the catalyst activity (62). All observation indicates that phosphorus plays different roles in different catalyst systems and, thus, shows in varied behavior toward deactivation. In our study on Mo_2N catalysts, it is very intriguing that phosphorus shows a promotion effect in enhancing the rates of both HDS and HDN reactions but a contrary performance against deactivation. This contrary behavior of phosphorus strongly suggests that the discrepancy most probably comes from the reactants that have a different affinity to phosphorus, although we cannot exclude the possibility that the H_2S and NH_3 produced exert different influences on HDN and HDS reactions. In HDN reaction, the addition of phosphorus seems favorable to the adsorption of organic nitrogen compounds and the breakage of C–N bonds, leading to improved activity. However, the activity is drastically reduced when phosphorus loses its effect due to the poison from the deposits of nitrogen compounds, especially at higher temperatures. In HDS reaction, similar to the observation in our previous investigation (40), phosphorus appears to help the formation of the bonds between Mo and N, and thus contributes to higher activity. Furthermore, its resistance against adsorption of sulfur compounds helps to maintain the catalytic activity of Mo_2N catalysts.

CONCLUSIONS

Mo_2N is an effective catalyst for HDS of benzothiophene. Ethylbenzene is the exclusive product over the whole temperature range investigated. Adding P_2O_5 to the precursor MoO_3 improved the activity of Mo_2N catalysts in HDS of benzothiophene as well as their resistance against catalyst deactivation. The reaction pathway of HDS appears unchanged by adding phosphorus. The bulk structure of face-centered-cubic Mo_2N and its morphology are retained after HDS reaction. However, adding phosphorus to the precursor results in growing polycrystallinity and amorphism in Mo_2N catalysts. A great amount of sulfur compounds are found deposited on the surface of the catalysts after reaction, which appears to lead to catalyst deactivation.

REFERENCES

1. Gates, B. C., Katzer, J. R., and Schuit, G. C. A., "Chemistry of Catalytic Processes," McGraw–Hill, New York, 1979.
2. Topsøe, H., and Clausen, B. S., *Catal. Rev.-Sci. Eng.* **26**, 3 (1985).
3. Prins, R., De Beer, V. H. J., and Somorjai, G. A., *Catal. Rev.-Sci. Eng.* **31**, 1 (1989).
4. Startsev, A. N., *Catal. Rev.-Sci. Eng.* **37**, 3 (1995).
5. Cruz Reyes, J., Avalos-Borja, M., Lopez Cordero, R., and Lopez Agudo, A., *Appl. Catal. A* **120**, 147 (1994).
6. Okamoto, Y., Gomi, I., Mori, Y., Imanaka, T., and Teranishi, S., *React. Kinet. Catal. Lett.* **22**, 417 (1983).
7. Lewis, J. M., and Kydd, R. A., *J. Catal.* **136**, 478 (1992).
8. Eijsbout, S., Van Gestel, J. N. M., Van Veen, J. A. R., De Beer, V. H. R., and Prins, R., *J. Catal.* **131**, 412 (1991).
9. Colling, C. W., and Thompson, L. T., *J. Catal.* **146**, 193 (1994).
10. Goldwasser, J., Fang, S. M., Houalla, M., and Hall, W. K., *J. Catal.* **115**, 34 (1989).
11. Ramirez, J., Castano, V. M., Leclercq, C., and Lopez Agudo, A., *Appl. Catal. A* **83**, 251 (1992).
12. Eberly, P. E., Jr., U.S. Patent 4,003,828 (1977).
13. Pine, L. A., U.S. Patent 3,904,550 (1975).
14. Wilson, G., and Kayamote, M., U.S. Patent 4,388,222 (1983).
15. Millman, W. S., U.S. Patent 4,392,985 (1983).
16. Mickelson, G. A., U.S. Patents 3,749,663; 3,755,196; 3,755,150; 3,775,148; (1973).
17. Fitz, C. W., and Rase, H. F., *Ind. Eng. Chem. Prod. Res. Dev.* **22**, 40 (1983).
18. Lopez Cordero, R., Esquivel, N., Lazaro, J., Fierro, J. L. G., and Lopez Agudo, A., *Appl. Catal.* **48**, 341 (1989).
19. Mangnus, P. J., Van Veen, J. A. R., Eijsbouts, S., De Beer, V. H. J., and Moulijn, J. A., *Appl. Catal.* **61**, 99 (1990).
20. Lewis, J. M., Kydd, R. A., Boorman, M., and Van Rhyn, P. H., *Appl. Catal. A* **84**, 103 (1992).
21. Stanislaus, A., Abi-halabi, M., and Al-Dolama, K., *Appl. Catal.* **39**, 239 (1988).
22. Ramirez, J., Castano, V. M., Leclercq, C., and Lopez Agudo, A., *Appl. Catal.* **83**, 251 (1992).
23. Fierro, J. L. G., Lopez Agudo, A., Esquivel, N., and Lopez Cordero, R., *Appl. Catal.* **48**, 353 (1989).
24. Sajkowski, D. J., Miller, J. T., Zajac, G. W., Morrison, T. I., Chen, H., and Fazzini, D. R., *Appl. Catal.* **62**, 205 (1990).
25. Chadwick, D., Aitchison, D. W., Badilla Ohlbaum, R., and Josefsson, L., *in* "Preparation of Catalysts III, Studies in Surface Science and Catalysis" (G. Poncelet, P. Grange, and P. A. Jacobs, Eds.), Vol. 16, p. 323. Elsevier, Amsterdam, 1983.
26. Vissers, J. P. R., Scheffer, B., De Beer, V. H. J., Moulijn, J. A., and Prins, R., *J. Catal.* **105**, 277 (1987).
27. Volpe, L., and Boudart, M., *J. Solid State Chem.* **59**, 332 (1985).
28. Volpe, L., and Boudart, M., *J. Solid State Chem.* **59**, 348 (1985).
29. Lee, J. S., Oyama, S. T., and Boudart, M., *J. Catal.* **106**, 125 (1987).
30. Lee, J. S., and Boudart, M., *Appl. Catal.* **19**, 207 (1985).

31. Schlatter, J. C., Oyama, S. T., Metcalfe, J. E., and Lambert, J. M., *Ind. Eng. Chem. Res.* **27**, 1648 (1988).
32. Markel, E. J., and Zee, J. W., *J. Catal.* **126**, 643 (1990).
33. Abe, H., and Bell, A. T., *Catal. Lett.* **18**, 1 (1993).
34. Nagai, M., Miyao, T., and Tuboi, T., *Catal. Lett.* **18**, 9 (1993).
35. Choi, J. G., Brenner, J. R., and Thompson, L. T., *J. Catal.* **154**, 33 (1995).
36. Choi, J. G., Brenner, J. R., Colling, C. W., Demczyk, B. G., Dunning, J. L., and Thompson, L. T., *Catal. Today* **15**, 201 (1992).
37. Raje, A., Liaw, S. J., Chary, K. V. R., and Davis, B. H., *Appl. Catal. A* **123**, 229 (1995).
38. Liaw, S. J., Raje, A., Chary, K. V. R., and Davis, B. H., *Appl. Catal. A* **123**, 251 (1995).
39. Li, S., and Lee, J. S., *J. Catal.* **162**, 76 (1996).
40. Li, S., and Lee, J. S., *J. Catal.* **173**, 134 (1998).
41. Barrett, E. P., Joyner, L. G., and Halenda, P. P., *J. Amer. Chem. Soc.* **73**, 373 (1951).
42. Harvath, G., and Kawazoe, K., *J. Chem. Eng. Jpn.* **16**, 470 (1983).
43. Halsey, G. D., *J. Amer. Chem. Soc.* **16**, 931 (1948).
44. Lowell, S., and Shields, J. E., "Powder Surface Area and Porosity," 3rd ed. Chapman & Hall, London/New York 1993.
45. Briggs, D., and Seah, M. P., "Practical Surface Analysis. Vol. 1. Auger and X-ray Photoelectron Spectroscopy," p. 562. Wiley, New York, 1990.
46. Brunauer, S., Demming, L. S., Demming, W. S., and Teller, E., *J. Amer. Chem. Soc.* **62**, 1723 (1940).
47. De Boer, J. H., *in* "The Structure and Properties of Porous Materials" (D. H. Everett and F. S. Stone, Eds.), J. Colloid Interface Sci., Vol. 62, p. 1723. Academic Press, New York, 1958.
48. Weisz, P. B., and Prater, C. D., *Adv. Catal. Rel. Sub.* **6**, 143 (1954).
49. Moulder, J. F., Stickle, W. F., Sobol, P. E., and Bomben, K. D., "Handbook of X-ray Photoelectron Spectroscopy," Perkin-Elmer, Eden Prairie, MN, 1992.
50. Alstrup, I., Chorkendorff, I., Candia, R., Clausen, B. S., and Topsøe, H., *J. Catal.* **77**, 393 (1982).
51. Brown, J. R., and Ternan, M., *Ind. Eng. Chem. Prod. Res. Dev.* **23**, 557 (1984).
52. Woo, H. C., Nam, I., Lee, J. S., Chung, J. S., Lee, K. H., and Kim, Y. G., *J. Catal.* **138**, 525 (1992).
53. Suzuki, K., Soma, M., Onishi, T., and Tamaru, K., *J. Electron Spectrosc. Relat. Phenom.* **24**, 283 (1981).
54. Patterson, T. A., Carver, J. C., Leyden, D. E., and Jercules, D. M., *J. Phys. Chem.* **80**, 1702 (1976).
55. Grim, S. O., and Matienzo, L. J., *Inorg. Chem.* **14**, 1014 (1975).
56. Lee, J. S., *Korean J. Chem. Eng.* **6**, 196 (1989).
57. Portela, L., Grange, P., and Delmon, B., *J. Catal.* **156**, 243 (1995).
58. Gellman, A. J., Neiman, D., and Somorjai, G. A., *J. Catal.* **107**, 92 (1987).
59. Gellman, A. J., Bussell, M. E., and Somorjai, G. A., *J. Catal.* **107**, 103 (1987).
60. Voorhies, J. D., U.S. Patent 4,082,652 (1978).
61. Bouwens, S. M. A. M., Vissers, J. P. R., De Beer, V. H. J., and Prins, R., *J. Catal.* **112**, 401 (1988).
62. Colgan, J. D., and Chomitz, N., U.S. Patent 3,287,280, 1966.